Scaling Wide Residual Networks for Panoptic Segmentation

Liang-Chieh Chen[1]   Huiyu Wang[2*]   Siyuan Qiao[2*]

[1]Google Research

[2]Johns Hopkins University

Abstract

The Wide Residual Networks (Wide-ResNets), a shallow but wide model variant of the Residual Networks (ResNets) by stacking a small number of residual blocks with large channel sizes, have demonstrated outstanding performance on multiple dense prediction tasks. However, since proposed, the Wide-ResNet architecture has barely evolved over the years. In this work, we revisit its architecture design for the recent challenging panoptic segmentation task, which aims to unify semantic segmentation and instance segmentation. A baseline model is obtained by incorporating the simple and effective Squeeze-and-Excitation and Switchable Atrous Convolution to the Wide-ResNets. Its network capacity is further scaled up or down by adjusting the width (i.e., channel size) and depth (i.e., number of layers), resulting in a family of SWideRNets (short for Scaling Wide Residual Networks). We demonstrate that such a simple scaling scheme, coupled with grid search, identifies several SWideRNets that significantly advance state-of-the-art performance on panoptic segmentation datasets in both the fast model regime and strong model regime.

1. Introduction

Computer vision systems have achieved remarkable performance across a wide range of image recognition tasks, including image classification [46, 79], object detection [22, 73], and dense prediction [62, 5], thanks to the recent advances in learning algorithms [23] (*e.g.*, better optimizer [42], normalization techniques [40, 76, 92, 71], and scalable training systems [1, 24, 67]). The improvement of neural network architectures especially plays an important role, as manifested on public benchmarks [19, 57, 75].

Gaining in popularity for its simplicity and effectiveness, Residual Networks (ResNets) [28] have been the building blocks of many modern neural network architectures [105, 97, 36, 95, 54, 21, 72, 106]. Specifically, the Wide-ResNets [105] adopt the 'shallow but wide' architec-

(a) PQ *vs*. inference time (ms) on COCO val set.

(b) PQ *vs*. inference time (ms) on Cityscapes Vistas val set
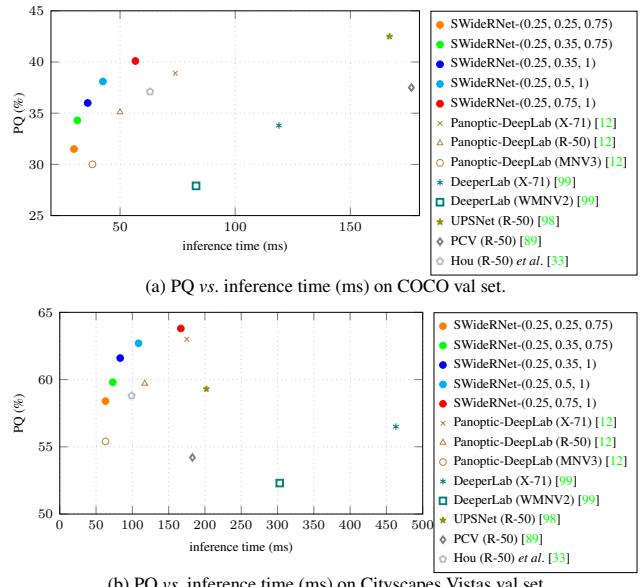
Figure 1. PQ *vs*. GPU inference time. Our fast SWideRNet model variants, deployed as the network backbone in Panoptic-DeepLab [12], significantly improve the speed-accuracy trade-off.

ture design (*i.e.*, fewer layers but with large channels) and show superior performance over the 'deep but thin' architectures (*i.e.*, more layers but with small channels). Along the same direction, the Wide-ResNet-38 (WR-38) [95], a sophisticated human-designed wide residual network, is one of the top-performing network backbones on many dense prediction benchmarks [14, 64]. However, since proposed in 2016, the architecture of WR-38 has barely evolved over the years. Recently, a simple modification of WR-38, by altering the last two residual blocks, leads to a slightly better and faster architecture WR-41 [4], when deployed as the network backbone in Panoptic-DeepLab [12] framework. The resulting model has shown state-of-the-art performance for panoptic segmentation [44], which is a challenging dense prediction task with the goal to unify semantic segmentation [30] and instance segmentation [26].

In this work, we ask if we may revisit the architecture design of wide residual networks to further boost the panoptic

---

*Work done while an intern at Google.

segmentation performance and even improve the model inference speed. In particular, a baseline model is obtained by equipping the WR-41 [4] with the simple and effective modules, Squeeze-and-Excitation (SE) [36] and Switchable Atrous Convoloution (SAC) [70]. Similar to [105, 35, 86], its network capacity could be further adjusted by three scaling factors (w_1, w_2, ℓ), where w_1 controls the channel size of the first two stages of a network backbone, while w_2 and ℓ adjust the network width (*i.e.*, channel size) and depth (*i.e.*, number of layers) of the remaining stages, respectively. The resulting model SWideRNet-(w_1, w_2, ℓ) (short for **S**caling **W**ide **R**esidual Network with scaling factors (w_1, w_2, ℓ)) is deployed as the network backbone in Panoptic-DeepLab [12] framework.

The SWideRNet-(w_1, w_2, ℓ) defines a large number of backbone architectures, targeting for different applications. The search space for those three scaling factors is discretized, allowing us to employ the simple and effective grid search method. Two model regimes are considered in this work, where the first one contains fast model variants and the other contains strong architectures. As a result, our main contribution lies in empirically identifying several fast SWideRNet backbones that attain state-of-the-art speed-accuracy trade-off, as well as several strong SWideRNet backbones that further push the envelope of panoptic segmentation benchmarks. As shown in Fig. 1, our fast SWideRNets attain a better speed-accuracy trade-off than prior state-of-the-art models, showing at least 3% PQ better than the MobileNetv3 [34] backbone at a similar speed. Interestingly, the found fast SWideRNets all share the same scaling factor $w_1 = 0.25$, indicating that the first two stages of Wide-ResNets are the speed bottleneck. Finally, for the strong model regime, we found that going deeper (*i.e.*, only increasing ℓ) is the most efficient strategy to scale up the network capacity, suggesting that the Wide-ResNets may be already sufficiently 'wide'. Our strong SWideRNet model variants consistently outperform prior *bottom-up* state-of-the-art Axial-DeepLab [90] on three datasets. Additionally, our *single* model outperforms ensemble models on Mapillary Vistas and ADE20K.

2. Related Works

Convolutional Neural Networks: Convolutional Neural Networks (CNNs) [48] deployed in a fully convolutional manner (FCNs [78, 62]) have achieved remarkable performance on dense prediction tasks. The improvement of neural network design is one of the main driving forces for state-of-the-art systems, from AlexNet [46], VGG [79], Inception [40, 83, 82], ResNet [28, 29] to more recent architectures, such as DenseNet [37], Xception [13, 69], and EfficientNet [86]. Due to the simple yet effective design of residual networks [28], there are many modern neural networks that build on top of it, including Wide-

ResNet [105, 95], ResNeXt [97], SENet [36], SKNet [54] Res2Net [21], RegNet [72], and ResNeSt [106].

Scaling CNNs: The capacity of Convolutional Neural Networks (CNNs) could be scaled up by stacking more convolutional layers or increasing the channels. ResNet [28] is the first work that successfully stacks over 1000 convolutional layers for small-resolution images, while PSPNet [107] employs ResNet with 269 layers, and shows outstanding semantic segmentation results. MobileNets [35, 77, 34] and ShuffleNets [63, 63] introduce a universal scaling factor to adjust network channels. Wide-ResNet [105, 95], GPipe [39], and BiT [45] explore scaling up both layers and channels for image classification. Auto-DeepLab [58] increases the channels of a base network for better semantic segmentation performance. More recently, EfficientNet [86] and EfficientDet [87] adopt a compound factor to effectively and simultaneously scaling up layers, channels, and input resolutions for image classification and object detection, respectively. Our model follows the same direction by scaling the architecture of Wide-ResNet [105, 95], specifically targeting for panoptic segmentation [44].

Panoptic Segmentation: State-of-the-art panoptic segmentation systems could be roughly categorized into top-down (or proposal-based) and bottom-up (or box-free) approaches. Top-down approaches [43, 68, 51, 55, 61, 98, 52, 10, 47, 93, 94] typically pair Mask R-CNN [27] with a light-weight 'stuff' segmentation branch, while bottom-up approaches [99, 20, 89, 12, 90] group 'thing' pixels from semantic segmentation predictions. Recently, Panoptic-DeepLab [12], a simple yet effective bottom-up system for panoptic segmentation, employs DeepLab semantic segmentation outputs [6, 8] coupled with a class-agnostic instance segmentation branch involving a simple instance center regression [41, 88, 65]. Panoptic-DeepLab [11] has achieved state-of-the-art results on several benchmarks, and our method builds on top of it.

3. Methods

In this section, we describe how to effectively scale the capacity of our baseline model, obtained by incorporating to Wide-ResNet-41 (WR-41) [105, 95, 4] the simple yet effective Squeeze-and-Excitation [36] and Switchable Atrous Convolution [70] modules. The resulting network family with different scaling factors is then explored for both fast model regime and strong model regime.

3.1. The SWideRNet family

Baseline model: The Wide Residual Networks [105, 95] have demonstrated outstanding performance on image classification [75], object detection [57], and semantic segmentation [19]. Specifically, the Wide-ResNet-38 (WR-38) [95], refined by several human-crafted networks with extensive experiments, has been the *de facto* network back-

(a) Squeeze-and-Excitation	(b) Switchable Atrous Convolution
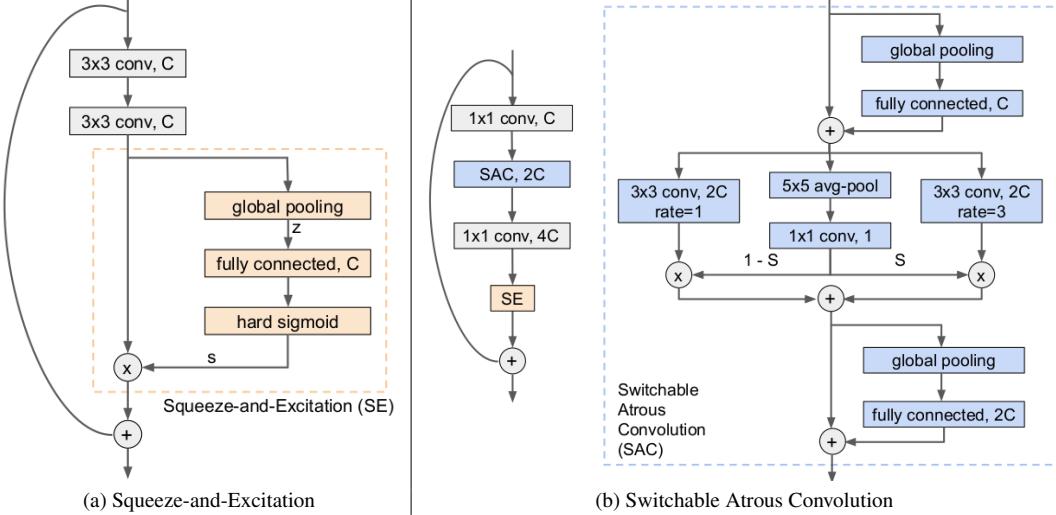
Figure 2. Illustration of our employment of (a) Squeeze-and-Excitation (SE) module and (b) Swithcable Atrous Convolution (SAC).

bone for semantic segmentation [64, 74, 109, 84, 53], and instance segmentation [56, 32] on Cityscapes leaderboard [14]. Recently, Chen *et al*. [4] attain state-of-the-art panoptic segmentation performance [44] on Cityscapes [14] by employing the Wide-ResNet-41 (WR-41), which improves both accuracy and speed over the WR-38 [95] (when deploying in the Panoptic-DeepLab [12] framework) by (1) removing the last residual block, and (2) repeating the second last residual block two more times.

Building on top of WR-41, we further incorporate the simplified Squeeze-and-Excitation (SE) module [36, 50] (where only one fully connected layer is used), and the Switchable Atrous Convolution (SAC) [70], forming our baseline model. In Fig. 2, we visualize the simplified SE module and SAC operation. To be concrete, the channel attention map $\mathbf{s}$ in the SE module is computed as follows.

$$\mathbf{s} = \sigma(W\mathbf{z}), \tag{1}$$

where $\mathbf{z}$ is the globally average-pooled input feature map, and W are the weights of a fully connected layer. Following [34], we employ the hard sigmoid function [15]: $\sigma(x) = \frac{ReLU6(x+3)}{6}$.

The SAC operation essentially gathers features computed with different atrous rates [31, 66, 5]. Specifically, we use $\mathbf{y} = \mathbf{Conv}(\mathbf{x}, \mathbf{w}, r)$ to denote the convolutional operation with weights $\mathbf{w}$, atrous rate r, input $\mathbf{x}$, and output $\mathbf{y}$. SAC adopts a switch function $\mathbf{S}$ to merge two feature maps:

$$(1 - \mathbf{S}(\mathbf{x})) \cdot \mathbf{Conv}(\mathbf{x}, \mathbf{w}, 1) + \mathbf{S}(\mathbf{x}) \cdot \mathbf{Conv}(\mathbf{x}, \mathbf{w}, 3), \tag{2}$$

where we use $r = 1$ and 3 for two convolutions (with weights $\mathbf{w}$ shared). The switch function $\mathbf{S}$ is input- and location-dependent. It is implemented as a 5×5 average pooling followed by a 1×1 convolution. Following [70], we also insert

two global context modules before and after the main operation of SAC. Those global context modules are lightweight and are implemented as global average pooling followed by a fully connected layer. We use ordinary convolution in the SAC operation (*i.e*., no deformation [17]).

Scaling factors: Similar to [105, 35, 86], we adopt scaling factors, (w_1, w_2, ℓ), to scale the network capacity of our baseline model, where w_1 scales the channels of the first two stages (denoted as conv1 and conv2), w_2 and ℓ scale the channels and layers of the remaining stages (denoted as conv3, conv4, conv5, and conv6), respectively. The resulting family of networks is dubbed SWideRNet-(w_1, w_2, ℓ) for **S**caling **W**ide **R**esidual Networks with scaling factors (w_1, w_2, ℓ). We illustrate the network architecture in Tab. 1. The total number of layers in the network backbone is thus equal to $7 + 33 \times \ell$. Note that this calculation does not include the SE and extra operations incurred by the SAC.

3.2. Exploring SWideRNet

The SWideRNet-(w_1, w_2, ℓ) family defines abundant network architectures. One thus could search for different SWideRNet architectures, designed for different objectives and applications. In this work, we apply SWideRNets to panoptic segmentation [44] for two scenarios. In the first scenario, we target at designing fast SWideRNets that attain state-of-the-art speed-accuracy trade-off (*i.e*., PQ *vs*. GPU runtime), which is applicable to on-device panoptic segmentation. The latency speed is directly measured by a GPU, instead of by any proxy (*e.g*., M-Adds). In the second scenario, we aim for state-of-the-art accuracy regardless of some costs (*e.g*., model parameters and speed), which could be deployed in cloud or server-side panoptic segmentation.

Grid search: The search space of SWideRNet-(w_1, w_2, ℓ) is discretized, allowing us to employ the sim-

stage	input size	output size	WR-41 [4]	SWideRNet-(w_1, w_2, ℓ)
conv1	224×224	112×112	3×3, 64, stride 2	3×3, 64×w_1, stride 2
conv2	112×112	56×56	$\begin{bmatrix} 3\times3,\ 128 \\ 3\times3,\ 128 \end{bmatrix}\times3$	$\begin{bmatrix} 3\times3,\ 128\times w_1 \\ 3\times3,\ 128\times w_1 \end{bmatrix}\times3$
			3×3 max-pool, stride 2	
conv3	56×56	28×28	$\begin{bmatrix} 3\times3,\ 256 \\ 3\times3,\ 256 \end{bmatrix}\times3$	$\begin{bmatrix} 3\times3,\ 256\times w_2 \\ 3\times3,\ 256\times w_2 \\ SE \end{bmatrix}\times3\ell$
conv4	28×28	14×14	$\begin{bmatrix} 3\times3,\ 512 \\ 3\times3,\ 512 \end{bmatrix}\times6$	$\begin{bmatrix} 3\times3,\ 512\times w_2 \\ 3\times3,\ 512\times w_2 \\ SE \end{bmatrix}\times6\ell$
conv5	14×14	7×7	$\begin{bmatrix} 3\times3,\ 1024 \\ 3\times3,\ 1024 \end{bmatrix}\times3$	$\begin{bmatrix} 3\times3,\ 1024\times w_2 \\ 3\times3,\ 1024\times w_2 \\ SE \end{bmatrix}\times3\ell$
conv6	7×7	7×7	$\begin{bmatrix} 1\times1,\ 512 \\ 3\times3,\ 1024 \\ 1\times1,\ 2048 \end{bmatrix}\times3$	$\begin{bmatrix} 1\times1,\ 512\times w_2 \\ 3\times3\ \text{SAC},\ 1024\times w_2 \\ 1\times1,\ 2048\times w_2 \\ SE \end{bmatrix}\times3\ell$
	7×7	1×1	average-pool, 1000-d fc, softmax	

Table 1. Architectures for our implementation of Wide-ResNet-41 (WR-41) and our SWideRNet-(w_1, w_2, ℓ) on ImageNet. SE denotes the simplified squeeze-and-excitation module (where only one fully connected layer is used) and SAC denotes the Switchable Atrous Convolution. Our SWideRNet scales the channels and layers of WR-41 to obtain a family of network backbones for panoptic segmentation. Note, if not specified, a strided convolution is used in the last residual block if spatial resolution changes.

ple yet effective grid search method. We elaborate on the discretized search space for each scenario below.

Fast mode regime: We constrain SWideRNet-(w_1, w_2, ℓ) to be in the search space $\boldsymbol{S}_{fast}$ by scaling down the network capacity for fast inference speed, resulting in a total of only 45 architecture candidates.

$$\begin{aligned} \boldsymbol{S}_{fast} = \{(w_1, w_2, \ell)| & w_1 \in \{0.25, 0.5, 1\}, \\ & w_2 \in \{0.25, 0.35, 0.5, 0.75, 1\}, \\ & \ell \in \{0.35, 0.75, 1\}\}, \end{aligned} \quad (3)$$

Strong model regime: We scale up the network capacity for better prediction accuracy by considering SWideRNet-(w_1, w_2, ℓ) in the search space $\boldsymbol{S}_{strong}$, resulting in a total of 21 architecture candidates. In practice, we only experiment with 11 candidates since not all the candidates could fit into the GPU/TPU memories.

$$\begin{aligned} \boldsymbol{S}_{strong} = \{(w_1, w_2, \ell)| & w_1 \in \{1\}, \\ & w_2 \in \{1, 1.5, 2\}, \\ & \ell \in \{1, 2, 3, 4, 5, 5.5, 6\}\}, \quad (4) \end{aligned}$$

4. Experimental Results

We conduct experiments on several datasets.

COCO [57]: There are 118K, 5K, and 20K images for training, validation, and testing, respectively. The dataset consists of 80 'thing' and 53 'stuff' classes.

Cityscapes [14]: The dataset consists of 2975, 500, and 1525 traffic-related images for training, validation, and testing, respectively. It contains 8 'thing' and 11 'stuff' classes.

Mapillary Vistas [64]: A large-scale traffic-related dataset, containing 18K, 2K, and 5K images for training, validation and testing, respectively. It contains 37 'thing' classes and 28 'stuff' classes in a variety of image resolutions, ranging from 1024×768 to more than 4000×6000

ADE20K [108]: A high-quality densely annotated dataset, consisting of 20K, 2K, and 3K images for training, validation and testing, respectively. There are 100 'thing' and 50 'stuff' classes.

Experimental setup: We report mean IoU, average precision (AP), and panoptic quality (PQ) to evaluate the semantic, instance, and panoptic segmentation results.

Our proposed SWideRNet is employed as the backbone in Panoptic-DeepLab [12]. We follow closely the experimental setup of [12]. For example, all our models are trained using TensorFlow [1] on 32 TPUs with the 'poly' learning rate policy [60] and an initial learning rate of 0.0001. We fine-tune the batch normalization [40] parameters, perform random scale data augmentation during training, and optimize with Adam [42] without weight decay.

On COCO, our models are trained with crop size 641×641 and batch size 64. Few models are trained with crop size 1025×1025 for better accuracy and we will clearly specify it. On Cityscapes, we use crop size 1025×2049 and batch size 32, while on Mapillary Vistas, the images are

	Op 1	Prob	Mag	Op 2	Prob	Mag
Sub-policy 1	Sharpness	0.4	1.4	Brightness	0.2	2.0
Sub-policy 2	Equalize	0	1.8	Contrast	0.2	2.0
Sub-policy 3	Sharpness	0.2	1.8	Color	0.2	1.8
Sub-policy 4	Solarize	0.2	1.4	Equalize	0.6	1.8
Sub-policy 5	Sharpness	0.2	0.2	Equalize	0.2	1.4

Table 2. Augmentation policy used in our experiments. We refer readers to AutoAugment [16] for details of augmentation operations. Each sub-policy consists of two **Op**erations with different **Prob**abilities and **Mag**nitudes. During training, one of the sub-policies is selected uniformly at random.

MG	SAC	SE	Sep-Conv	PQ (%)	Params (M)	M-Adds (B)	Runtime (ms)
				39.6	147.32	655.66	101.16
✓				40.1	147.32	659.02	104.39
	✓			40.8	151.26	680.68	105.91
	✓	✓		41.4	168.77	680.79	108.36
	✓	✓	✓	41.2	136.92	499.16	88.48

Table 3. Design choices on COCO *val* set. The baseline corresponds to WR-41. **MG:** Multi-Grid. **SAC:** Switchable Atrous Convolution. **SE:** Squeeze-and-Excitation. **Sep-Conv:** Employing separable convolutions in ASPP and decoder modules.

resized to 2049 pixels at the longest side, and we randomly crop 1025×2049 patches during training with batch size 32. Finally, our model is trained with crop size 641×641 with batch size 64 on ADE20K.

We set training iterations to 500K, 60K, 500K, 180K for COCO, Cityscapes, Mapillary Vistas, and ADE20K, respectively. We employ the same loss functions and loss weights as Panoptic-DeepLab [12]. When training some of our large model variants, we adopt AutoAugment [16] with the augmentation policy defined in Tab. 2.

During evaluation, due to the sensitivity of PQ [98, 51, 68], we re-assign to 'VOID' label all 'stuff' segments whose areas are smaller than a threshold. The thresholds on COCO, Cityscapes, Mapillary Vistas, and ADE20K are 4096, 2048, 4096, and 4096, respectively. Additionally, we adopt multi-scale inference (scales equal to $\{0.5, 0.75, 1, 1.25, 1.5\}$ for COCO and ADE20K, and $\{0.5, 0.75, 1, 1.25, 1.5, 1.75, 2\}$ for Cityscapes and Mapillary Vistas) and left-right flipped inputs.

4.1. Ablation Studies

We perform ablation studies on the validation set of COCO panoptic segmentation.

Design choices: Our system builds on top of Panoptic-DeepLab [12] by deploying different backbone architectures. In Tab. 3, we report the effect of incorporating new modules to our baseline, Wide-ResNet-41 (WR-41) [4]. Adopting the multi-grid scheme [7, 91] in the last three residual blocks (with unit rate $\{1, 2, 4\}$, same as [7]) improves the performance by 0.5% PQ with extra marginal computation overhead (but no extra parameters). However, it is more effective to employ the Switchable Atrous Convolution (SAC) [70] in the last three residual blocks, which improves over the baseline by 1.2% PQ with small computational overhead. Additionally, adding Squeeze-and-Excitation (SE) modules could further improve the performance by 0.6% PQ. Finally, we notice that employing separable convolutions [35] in the ASPP and decoder modules, same as the original design of Panoptic-DeepLab [12], only degrades the performance by 0.2% PQ while the inference speed is significantly improved. Therefore, for the fast model regime, we employ separable convolutions in the

ASPP and decoder modules, while original convolutions are used for the strong model regime.

Training tricks: During training, we employ drop path [38] with a constant survival rate 0.8, and AutoAugment [16] with policy defined in Tab. 2, which improve 0.2% PQ, and 0.3% PQ, respectively. Note that in all the reported experimental results, we only apply AutoAugment to the strongest model for test server evaluation.

Fast model regime: We conduct grid search in the fast model regime with search space defined by Eq. (3) where the channels and layers are scaled *down* for faster inference. Fig. 3 (a) shows the scatter plot of PQ *vs.* GPU inference time (Tesla V100-SXM2). We pinpoint five candidate architectures (marked in orange) that attain the best speed-accuracy trade-off, as shown in Fig. 3 (b). The found fast architectures share the same scaling factor $w_1 = 0.25$, indicating that the stages conv1 and conv2 are the speed bottleneck. We report detailed comparison with other state-of-the-art models in the following Sec. 4.2.

Strong model regime: Similarly, we perform grid search in the strong model regime with search space defined by Eq. (4) where the channels and layers are scaled *up* for better accuracy. As shown in Tab. 4, we find that 'Going Deeper' (*i.e.*, increasing only layers ℓ) is more efficient than both 'Going Wider' (*i.e.*, increasing only channels w_2) and 'Going Wider and Deeper' (*i.e.*, increasing both channels w_2 and layers ℓ). The finding suggests that the Wide-ResNets may be already sufficiently 'wide' on current benchmarks. The SWideRNet-(1, 1, 5.5) attains the best accuracy with crop size 641×641. When the crop size is increased to 1025×1025, the SWideRNet-(1, 1, 4) further improves the performance to 45.3% PQ, but with a slower inference speed. This backbone is selected for COCO test-dev evaluation. Finally, we adopt the same 'Going Deeper' strategy on the other datasets for strong model regime.

4.2. Fast Model Regime

In Tab. 6, we compare our five fast SWideRNet model variants with other state-of-the-art models on both COCO and Cityscapes. We report the end-to-end runtime (*i.e.*, inference time from an input image to final panoptic segmentation result, including *all* operations such as merging semantic and instance segmentation). The inference speed is

Scaling Factors	PQ (%)	Params (M)	Speed (ms)
(0.25, 0.25, 0.75)	31.5	7.77	30.01
(0.25, 0.35, 0.75)	34.3	13.39	31.45
(0.25, 0.35, 1)	36.0	18.83	35.96
(0.25, 0.5, 1)	38.1	36.19	42.57
(0.25, 0.75, 1)	40.1	77.97	56.66

(a)   (b)
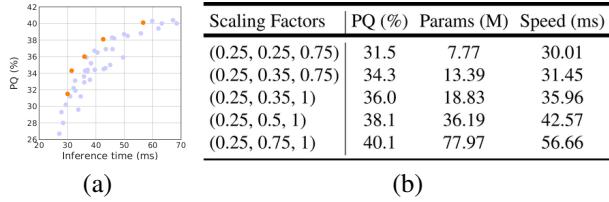
Figure 3. (a) Grid search for fast model variants. (b) Five selected fast SWideRNets (marked in orange in (a)).

Backbone	PQ (%)	Params (M)	M-Adds (B)	Runtime (ms)
Baseline Model				
SWideRNet-(1, 1, 1)	41.4	168.77	680.79	108.36
Going Wider				
SWideRNet-(1, 1.5, 1)	42.8	345.75	1205.95	175.84
SWideRNet-(1, 2, 1)	43.0	587.35	1925.75	266.85
Going Deeper				
SWideRNet-(1, 1, 2)	42.8	302.33	1119.77	190.37
SWideRNet-(1, 1, 3)	43.3	435.90	1558.75	310.90
SWideRNet-(1, 1, 4)	43.8	569.46	1997.73	407.88
SWideRNet-(1, 1, 5)	44.0	703.03	2436.71	452.42
SWideRNet-(1, 1, 5.5)	44.1	752.53	2614.01	504.66
SWideRNet-(1, 1, 5.5)†	44.4	752.53	2614.01	504.66
SWideRNet-(1, 1, 6)	44.0	836.59	2875.69	544.02
Going Wider and Deeper				
SWideRNet-(1, 1.5, 2)	43.7	646.22	2193.54	344.74
SWideRNet-(1, 1.5, 3)	44.1	946.69	3181.12	570.73
Going Deeper with Large Crop Size 1025×1025				
SWideRNet-(1, 1, 3)†	44.7	435.90	3911.58	641.21
SWideRNet-(1, 1, 4)†	45.3	569.46	5019.62	836.41

Table 4. Grid search for large models. † : Use AutoAugment.

measured on a Tesla V100-SXM2 GPU *with batch size of one*. Additionally, Fig. 1 shows the scatter plot of speed *vs*. accuracy. As shown in the table and figure, our models attain better speed-accuracy trade-off than all state-of-the-art models. Specifically, on the COCO dataset, employing our SWideRNet-(0.25, 0.35, 1) is 6% and 6.4% PQ better than using MobileNetv3 [34] as backbone in Panoptic-DeepLab [12] on *val* and *test-dev* set, respectively, while a similar inference speed is achieved. Using SWideRNet-(0.25, 0.5, 1) is 3% PQ better than ResNet-50 [28] on both *val* and *test-dev* sets, while our model is slightly faster. Finally, adopting our SWideRNet-(0.25, 0.75, 1) achieves a similar performance to Xception-71 [13, 69] (with 1025×1025 input) but with 2.3 times faster inference speed. On the Cityscapes dataset, when considering a similar inference speed, using our SWideRNet-(0.25, 0.25, 0.75) is 3% and 2.5% PQ better than using MobileNetv3 on *val* and *test* set, respectively. Employing SWideRNet-(0.25, 0.5, 1) is also 3% and 2.8% PQ better than ResNet-50 on *val* and *test* set, respectively. Our SWideRNet-(0.25, 0.75, 1) is also slightly faster and better than Xception-71.

More fast model results on Cityscapes: Our methods build on top of Panoptic-DeepLab [12], simultaneously generating semantic segmentation, instance segmentation, and panoptic segmentation results (*i.e.*, no need for specific task fine-tuning). Therefore, in Tab. 5, we additionally report the instance segmentation and semantic segmentation results for our fast model variants, evaluated on both Cityscapes validation and test sets [14].

4.3. Strong Model Regime

For the strong model regime, we adopt the "Going Deeper" strategy (*i.e.*, only scaling up the number of layers). We report the results for each dataset below.

COCO: Tab. 7 summarizes our *val* set results. Our SWideRNet-(1, 1, 4) without multi-scale inference already outperforms Aixal-DeepLab [90]. Incorporating the multi-scale inference further improves the performance to 45.8% PQ. In Tab. 8, our SWideRNet-(1, 1, 4) achieves 46.7% PQ on *test-dev*, outperforming the current *bottom-up* state-of-the-art Axial-DeepLab-L [90] by 2.5% PQ. Note that for this result, we increase the magnitudes of employed AutoAugment policy (Tab. 2) by a factor of 5, which additionally improves the performance by 0.2% PQ.

Cityscapes: As shown in Tab. 9, when using multi-scale inference, our SWideRNet-(1, 1, 4.5) outperforms Axial-DeepLab-XL [90] by 2.4% PQ (4.9% AP) with only Cityscapes fine annotations, and 1.1% PQ (2.6% AP) with extra Mapillary Vistas pretraining [64]. We then report the test set results in Tab. 10. When only using Cityscapes fine annotations, our model significantly outperforms current state-of-the-art Axial-DeepLab-XL [90] by 2% PQ and 4% AP. When using extra data [64], our model achieves 67.8% PQ, 42.2% AP, and 84.1% mIOU, better than Axial-DeepLab-XL [90] by 1.2% PQ and 2.6% AP. Following Naive-Student [4], with additional pseudo-labels [49, 109, 96] from Cityscapes video and train-extra sets, our model reaches the performance of 68.5% PQ and 43.4% AP, setting a new state-of-the-art.

Mapillary Vistas: Tab. 11 summarizes our *val* set results. Our SWideRNet-(1, 1, 4.5), with multi-scale inference, attains 44.8% PQ, 22.2% AP, and 60.0% mIoU, outperforming the *bottom-up* (or box-free) method Axial-DeepLab-L [90] by 3.7% PQ, 5.0% AP, and 1.6% mIoU. Remarkably, our *single* model even performs better than the ensemble of six Panoptic-DeepLab models [12] by 2.6% PQ, 4.0% AP, and 1.3% mIoU.

ADE20K: In Tab. 12, we report our results on ADE20K. On the *val* set, our SWideRNet-(1, 1, 4) significantly outperforms BGRNet [93] by 6% PQ and Auto-Panoptic [94] by 5.4% PQ. Additionally, our model achieves 49.96% mIoU and 83.78% Pixel-accuracy. On the test set, our *single* model yields the score of 59.14% (average of mIoU and Pixel-accuracy), 1.9% better than the ensemble of PSP-Nets [107], setting a new state-of-the-art. Interestingly, our SWideRNet-(1, 1.5, 3) achieves a higher score of

Method	Backbone	Input Size	PQ [val]	AP [val]	mIoU [val]	PQ [test]	AP [test]	mIoU [test]	Speed (ms)	M-Adds (B)
Panoptic-DeepLab	SWideRNet-(0.25, 0.25, 0.75)	1025 × 2049	58.4	30.2	77.6	56.6	25.5	76.9	63.05	151.97
Panoptic-DeepLab	SWideRNet-(0.25, 0.35, 0.75)	1025 × 2049	59.8	31.3	79.4	58.2	27.3	78.6	73.14	229.49
Panoptic-DeepLab	SWideRNet-(0.25, 0.35, 1)	1025 × 2049	61.6	33.3	80.2	60.0	29.6	79.6	83.25	319.14
Panoptic-DeepLab	SWideRNet-(0.25, 0.5, 1)	1025 × 2049	62.7	35.2	80.3	60.8	30.5	79.8	108.58	576.83
Panoptic-DeepLab	SWideRNet-(0.25, 0.75, 1)	1025 × 2049	63.8	36.1	80.6	61.6	31.2	80.6	166.83	1199.85

Table 5. Cityscapes end-to-end runtime results, including merging semantic and instance segmentation. All numbers are obtained by (1) a single-scale input (batch size *one*) without flipping, and (2) built-in TensorFlow library without extra inference optimization. [val]: Performance on val set. [test]: Performance on test set. We report PQ, AP, and mIoU for panoptic, instance, and semantic segmentation.

Method	Backbone	Input Size	PQ [val]	PQ [test]	Speed (ms)	M-Adds (B)
		COCO				
DeeperLab [99]	W-MNV2	641 × 641	27.9	28.1	83	-
DeeperLab [99]	Xception-71	641 × 641	33.8	34.3	119	-
Hou *et al.* [33]	ResNet-50	800 × 1333	37.1	-	63	-
PCV [89]	ResNet-50	800 × 1333	37.5	37.7	176.5	-
Panoptic-DeepLab [12]	MobileNetv3	641 × 641	30.0	29.8	38	12.24
Panoptic-DeepLab [12]	ResNet-50	641 × 641	35.1	35.2	50	77.79
Panoptic-DeepLab [12]	Xception-71	641 × 641	38.9	38.8	74	109.21
Panoptic-DeepLab [12]	Xception-71	1025 × 1025	39.7	39.6	132	279.25
UPSNet [98]	ResNet-50	800 × 1333	42.5	-	167	-
Panoptic-DeepLab	SWideRNet-(0.25, 0.25, 0.75)	641 × 641	31.5	31.7	30.01	31.67
Panoptic-DeepLab	SWideRNet-(0.25, 0.35, 0.75)	641 × 641	34.3	34.4	31.45	47.13
Panoptic-DeepLab	SWideRNet-(0.25, 0.35, 1)	641 × 641	36.0	36.2	35.96	64.98
Panoptic-DeepLab	SWideRNet-(0.25, 0.5, 1)	641 × 641	38.1	38.2	42.57	116.37
Panoptic-DeepLab	SWideRNet-(0.25, 0.75, 1)	641 × 641	40.1	40.3	56.66	240.59
		Cityscapes				
PCV [89]	ResNet-50	1024 × 2048	54.2	-	182.8	-
DeeperLab [99]	W-MNV2 [77]	1025 × 2049	52.3	-	303	-
DeeperLab [99]	Xception-71	1025 × 2049	56.5	-	463	-
Hou *et al.* [33]	ResNet-50	1024 × 2048	58.8	-	99	-
UPSNet [98]	ResNet-50	1024 × 2048	59.3	-	202	-
Panoptic-DeepLab [12]	MobileNetv3	1025 × 2049	55.4	54.1	63	54.17
Panoptic-DeepLab [12]	ResNet-50	1025 × 2049	59.7	58.0	117	381.39
Panoptic-DeepLab [12]	Xception-71	1025 × 2049	63.0	60.7	175	547.49
Panoptic-DeepLab	SWideRNet-(0.25, 0.25, 0.75)	1025 × 2049	58.4	56.6	63.05	151.97
Panoptic-DeepLab	SWideRNet-(0.25, 0.35, 0.75)	1025 × 2049	59.8	58.2	73.14	229.49
Panoptic-DeepLab	SWideRNet-(0.25, 0.35, 1)	1025 × 2049	61.6	60.0	83.25	319.14
Panoptic-DeepLab	SWideRNet-(0.25, 0.5, 1)	1025 × 2049	62.7	60.8	108.58	576.83
Panoptic-DeepLab	SWideRNet-(0.25, 0.75, 1)	1025 × 2049	63.8	61.6	166.83	1199.85

Table 6. End-to-end runtime, including merging semantic and instance segmentation. All results are obtained by (1) a single-scale input without flipping, and (2) built-in TensorFlow library without extra inference optimization. **PQ [val]:** PQ (%) on val set. **PQ [test]:** PQ (%) on test(-dev) set.

Method	Backbone	MS	PQ (%)	PQTh (%)	PQSt (%)
DeeperLab [99]	Xception-71		33.8	-	-
SSAP [20]	ResNet-101	✓	36.5	-	-
PCV [89]	ResNet-50		37.5	40.0	33.7
Panoptic-DeepLab [12]	Xception-71	✓	41.2	44.9	35.7
Axial-DeepLab [90]	Axial-ResNet-L	✓	43.9	48.6	36.8
Panoptic-DeepLab	SWideRNet-(1, 1, 4)		45.3	51.5	36.1
Panoptic-DeepLab	SWideRNet-(1, 1, 4)	✓	45.8	51.0	38.0

Table 7. COCO *val* set. **MS:** Multi-scale inputs.

Method	Backbone	MS	PQ	PQTh	PQSt
Top-down (Box-based) panoptic segmentation methods					
TASCNet [51]	ResNet-50		40.7	47.0	31.0
Panoptic-FPN [43]	ResNet-101		40.9	48.3	29.7
DETR [3]	ResNet-101		46.0	-	-
AUNet [55]	ResNeXt-152		46.5	55.8	32.5
UPSNet [98]	DCN-101 [17]	✓	46.6	53.2	36.7
Li *et al.* [52]	DCN-101 [17]		47.2	53.5	37.7
SpatialFlow [9]	DCN-101 [17]	✓	47.3	53.5	37.9
SOGNet [101]	DCN-101 [17]	✓	47.8	-	-
DetectoRS [70]	ResNeXt-101	✓	49.6	57.8	37.1
Bottom-up (Box-free) panoptic segmentation methods					
DeeperLab [99]	Xception-71		34.3	37.5	29.6
SSAP [20]	ResNet-101	✓	36.9	40.1	32.0
PCV [89]	ResNet-50		37.7	40.7	33.1
Panoptic-DeepLab [12]	Xception-71	✓	41.4	45.1	35.9
AdaptIS [80]	ResNet-101	✓	42.8	53.2	36.7
Axial-DeepLab-L [90]	Axial-ResNet-L	✓	44.2	49.2	36.8
Panoptic-DeepLab	SWideRNet-(1, 1, 4)	✓	46.7	52.2	38.3

Table 8. COCO test-dev set. **MS:** Multi-scale inputs.

Model	Extra Data	MS	PQ	AP	mIoU
SSAP [20]		✓	61.1	37.3	-
AdaptIS [80]		✓	62.0	36.3	79.2
Panoptic-DeepLab w/ Xception-71 [12]			63.0	35.3	80.5
Panoptic-DeepLab w/ Xception-71 [12]		✓	64.1	38.5	81.5
Axial-DeepLab-XL [90]			64.4	36.7	80.6
Axial-DeepLab-XL [90]		✓	65.1	39.0	81.1
Panoptic-DeepLab w/ SWideRNet-(1, 1, 4.5)			66.4	40.1	82.2
Panoptic-DeepLab w/ SWideRNet-(1, 1, 4.5)		✓	67.5	43.9	82.9
SpatialFlow [9]	COCO	✓	62.5	-	-
Seamless [68]	MV		65.0	-	80.7
Panoptic-DeepLab w/ Xception-71 [12]	MV		65.3	38.8	82.5
Panoptic-DeepLab w/ Xception-71 [12]	MV	✓	67.0	42.5	83.1
Axial-DeepLab-XL [90]	MV		67.8	41.9	84.2
Axial-DeepLab-XL [90]	MV	✓	68.5	44.2	84.6
Panoptic-DeepLab w/ SWideRNet-(1, 1, 4.5)	MV		68.5	42.8	84.6
Panoptic-DeepLab w/ SWideRNet-(1, 1, 4.5)	MV	✓	69.6	46.8	85.3

Table 9. Cityscapes val set. **MS:** Multi-scale inputs. **C:** Cityscapes coarse annotation. **V:** Cityscapes video. **MV:** Mapillary Vistas.

50.35% mIoU on the validation set, but a lower score of 40.47% mIoU on the test set, presenting another challenge in ADE20K to avoid over-fitting large models.

5. Discussion

M-Adds *vs*. real inference speed: We empirically discover that M-Adds (Multiply-Adds) or FLOPs are a very rough proxy of real-world inference speed (*e.g*., Tab. 6), echoing the findings from [100, 85]. Therefore, it is more accurate to directly measure the inference latency on the target device [18, 2] for comparing the speed-accuracy trade-off between different network architectures.

Model parameters: Our SWideRNets, derived from the Wide-ResNets [105, 95], share the same issue about large model parameters. This could be potentially alleviated by pruning the networks [25, 100].

6. Conclusion

In this work, we present SWideRNet-(w_1, w_2, ℓ), a family of neural networks by scaling the width (*i.e*., channel
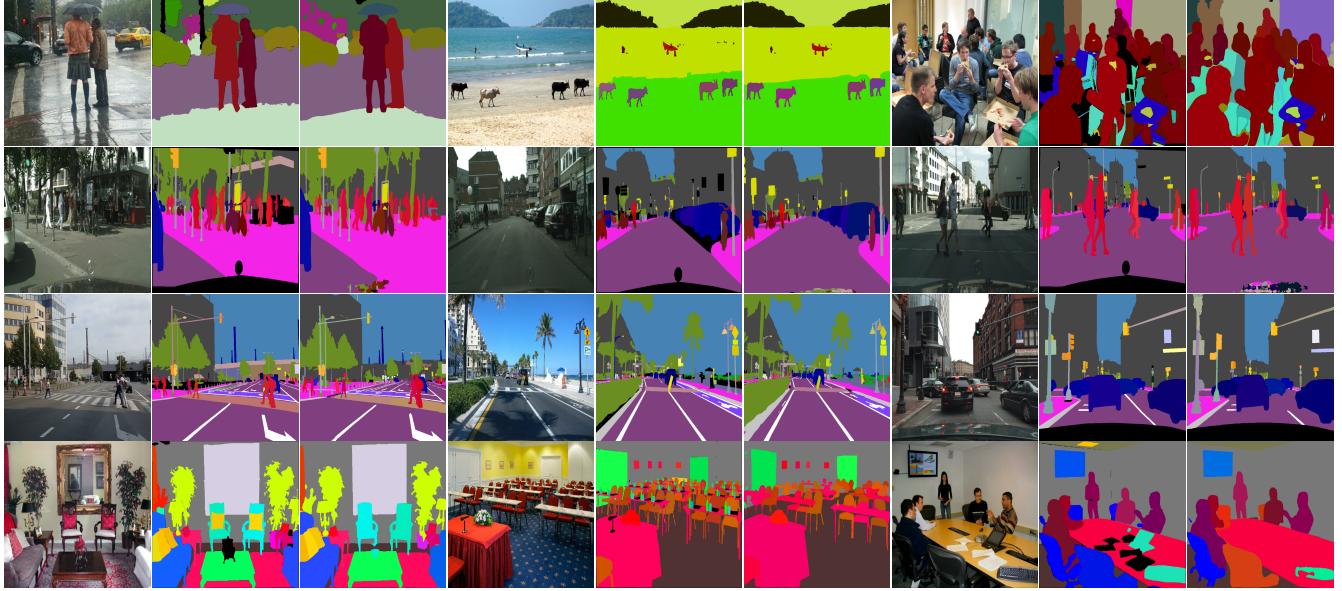
Figure 4. Our visualization results on COCO (1st row), Cityscsapes (2nd row), Mapillary Vistas (3rd row), and ADE20K (4th row). For every triple of images, we show (image, ground-truth, prediction). Our models struggle for small, thin, or heavily occluded objects.

Model	Extra Data	PQ	AP	mIoU
DecoupleSegNet [53]		-	-	82.8
Zhu *et al.* [109]	C, V, MV	-	-	83.5
DecoupleSegNet [53]	MV	-	-	83.7
HRNetV2 + OCR + SegFix [103, 104, 81]	C, MV	-	-	84.5
AdaptIS [80]		-	32.5	-
LevelSet R-CNN [32]		-	33.3	-
UPSNet [98]	COCO	-	33.0	-
PANet [59]	COCO	-	36.4	-
LevelSet R-CNN [32]	COCO	-	40.0	-
PolyTransform [56]	COCO	-	40.1	-
SSAP [20]		58.9	32.7	-
Li *et al.* [52]		61.0	-	-
Panoptic-DeepLab w/ Xception-71 [12]		62.3	34.6	79.4
Axial-DeepLab-XL [90]		62.8	34.0	79.9
TASCNet [51]	COCO	60.7	-	-
Seamless [68]	MV	62.6	-	-
Li *et al.* [52]	COCO	63.3	-	-
Panoptic-DeepLab w/ Xception-71 [12]	MV	65.5	39.0	84.2
Axial-DeepLab-XL [90]	MV	66.6	39.6	84.1
Naive-Student [4]	C†, V, MV	67.8	42.6	85.2
Panoptic-DeepLab w/ SWideRNet-(1, 1, 4.5)		64.8	38.0	80.4
Panoptic-DeepLab w/ SWideRNet-(1, 1, 4.5)	MV	67.8	42.2	84.1
Panoptic-DeepLab w/ SWideRNet-(1, 1, 4.5)	C†, V, MV	68.5	43.4	85.1

Table 10. Cityscapes test set. **C:** Cityscapes coarse annotation. **C†:** Cityscapes coarse images with pseudo-labels. **V:** Cityscapes video. **MV:** Mapillary Vistas.

Method	MS	PQ	PQTh	PQSt	AP	mIoU
Top-down (Box-based) panoptic segmentation methods						
TASCNet [51]		32.6	31.1	34.4	18.5	-
TASCNet [51]	✓	34.3	34.8	33.6	20.4	-
Seamless [68]		37.7	33.8	42.9	16.4	50.4
Bottom-up (Box-free) panoptic segmentation methods						
DeeperLab [99]		32.0	-	-	-	55.3
AdaptIS [80]		35.9	31.5	41.9	-	-
Panoptic-DeepLab (Auto-XL++ [58]) [12]	✓	40.3	-	-	16.9	57.6
Axial-DeepLab-L [90]		40.1	32.7	49.8	16.7	57.6
Axial-DeepLab-L [90]	✓	41.1	33.4	51.3	17.2	58.4
Panoptic-DeepLab (ensemble of 6 models) [12]	✓	42.2	-	-	18.2	58.7
Panoptic-DeepLab w/ SWideRNet-(1, 1, 4.5)		43.7	38.0	51.2	21.0	59.4
Panoptic-DeepLab w/ SWideRNet-(1, 1, 4.5)	✓	44.8	39.3	51.9	22.2	60.0

Table 11. Mapillary Vistas validation set. **MS:** Multiscale inputs.

Model	MS	Val set			Test set		
		PQ (%)	mIoU	Pixel-Acc	mIoU	Pixel-Acc	Score
BGRNet [93]		31.8	-	-	-	-	-
Auto-Panoptic [94]		32.4	-	-	-	-	-
PSPNet (single-model) [107]	✓	-	44.94	81.69	-	-	55.38
PSPNet (ensemble-model) [107]	✓	-	-	-	-	-	57.21
CPN [102]	✓	-	46.27	81.85	-	-	-
Panoptic-DeepLab w/ SWideRNet-(1, 1, 4)		37.53	49.37	83.50	-	-	-
Panoptic-DeepLab w/ SWideRNet-(1, 1, 4)	✓	37.86	49.96	83.78	42.09	76.19	59.14
Panoptic-DeepLab w/ SWideRNet-(1, 1.5, 3)		36.93	49.63	83.71	-	-	-
Panoptic-DeepLab w/ SWideRNet-(1, 1.5, 3)	✓	37.41	50.35	84.02	40.47	75.21	57.84

Table 12. ADE20K. **MS:** Multiscale inputs. **Score:** Average of mIoU and Pixel-Accuracy.

size) and depth (*i.e.*, number of layers) of Wide Residual Networks. Two search spaces are explored, where the first one contains fast model variants, and the other one contains strong architectures. Discretizing the search space allows us to employ the simple but effective grid search. As a result, we empirically identify several fast SWideRNets that attain outstanding performance in terms of speed-accuracy trade-off, and several strong SWideRNets that further advance sate-of-the-art results on several public benchmarks.

References

[1] Martín Abadi, Paul Barham, Jianmin Chen, Zhifeng Chen, Andy Davis, Jeffrey Dean, Matthieu Devin, Sanjay Ghemawat, Geoffrey Irving, Michael Isard, Manjunath Kudlur, Josh Levenberg, Rajat Monga, Sherry Moore, Derek G. Murray, Benoit Steiner, Paul Tucker, Vijay Vasudevan, Pete Warden, Martin Wicke, Yuan Yu, and Xiaoqiang Zheng. Tensorflow: A system for large-scale machine learning. In *Proceedings of the 12th USENIX Conference on Operating Systems Design and Implementation*, 2016. 1, 4

[2] Han Cai, Chuang Gan, Tianzhe Wang, Zhekai Zhang, and Song Han. Once-for-all: Train one network and specialize it for efficient deployment. In *ICLR*, 2020. 7

[3] Nicolas Carion, Francisco Massa, Gabriel Synnaeve, Nicolas Usunier, Alexander Kirillov, and Sergey Zagoruyko. End-to-end object detection with transformers. In *ECCV*, 2020. 7

[4] Liang-Chieh Chen, Raphael Gontijo Lopes, Bowen Cheng, Maxwell D Collins, Ekin D Cubuk, Barret Zoph, Hartwig Adam, and Jonathon Shlens. Naive-Student: Leveraging Semi-Supervised Learning in Video Sequences for Urban Scene Segmentation. In *ECCV*, 2020. 1, 2, 3, 4, 5, 6, 8

[5] Liang-Chieh Chen, George Papandreou, Iasonas Kokkinos, Kevin Murphy, and Alan L Yuille. Semantic image segmentation with deep convolutional nets and fully connected CRFs. In *ICLR*, 2015. 1, 3

[6] Liang-Chieh Chen, George Papandreou, Iasonas Kokkinos, Kevin Murphy, and Alan L Yuille. DeepLab: Semantic image segmentation with deep convolutional nets, atrous convolution, and fully connected CRFs. *IEEE TPAMI*, 2017. 2

[7] Liang-Chieh Chen, George Papandreou, Florian Schroff, and Hartwig Adam. Rethinking atrous convolution for semantic image segmentation. *arXiv:1706.05587*, 2017. 5

[8] Liang-Chieh Chen, Yukun Zhu, George Papandreou, Florian Schroff, and Hartwig Adam. Encoder-decoder with atrous separable convolution for semantic image segmentation. In *ECCV*, 2018. 2

[9] Qiang Chen, Anda Cheng, Xiangyu He, Peisong Wang, and Jian Cheng. Spatialflow: Bridging all tasks for panoptic segmentation. *arXiv:1910.08787*, 2019. 7

[10] Yifeng Chen, Guangchen Lin, Songyuan Li, Omar Bourahla, Yiming Wu, Fangfang Wang, Junyi Feng, Mingliang Xu, and Xi Li. Banet: Bidirectional aggregation network with occlusion handling for panoptic segmentation. In *CVPR*, 2020. 2

[11] Bowen Cheng, Maxwell D Collins, Yukun Zhu, Ting Liu, Thomas S Huang, Hartwig Adam, and Liang-Chieh Chen. Panoptic-DeepLab. In *ICCV COCO + Mapillary Joint Recognition Challenge Workshop*, 2019. 2

[12] Bowen Cheng, Maxwell D Collins, Yukun Zhu, Ting Liu, Thomas S Huang, Hartwig Adam, and Liang-Chieh Chen. Panoptic-DeepLab: A simple, strong, and fast baseline for bottom-up panoptic segmentation. In *CVPR*, 2020. 1, 2, 3, 4, 5, 6, 7, 8

[13] François Chollet. Xception: Deep learning with depthwise separable convolutions. In *CVPR*, 2017. 2, 6

[14] Marius Cordts, Mohamed Omran, Sebastian Ramos, Timo Rehfeld, Markus Enzweiler, Rodrigo Benenson, Uwe Franke, Stefan Roth, and Bernt Schiele. The cityscapes dataset for semantic urban scene understanding. In *CVPR*, 2016. 1, 3, 4, 6

[15] Matthieu Courbariaux, Yoshua Bengio, and Jean-Pierre David. Binaryconnect: Training deep neural networks with binary weights during propagations. In *NeurIPS*, 2015. 3

[16] Ekin D Cubuk, Barret Zoph, Dandelion Mane, Vijay Vasudevan, and Quoc V Le. Autoaugment: Learning augmentation policies from data. In *CVPR*, 2019. 5

[17] Jifeng Dai, Haozhi Qi, Yuwen Xiong, Yi Li, Guodong Zhang, Han Hu, and Yichen Wei. Deformable convolutional networks. In *ICCV*, 2017. 3, 7

[18] Jin-Dong Dong, An-Chieh Cheng, Da-Cheng Juan, Wei Wei, and Min Sun. Dpp-net: Device-aware progressive search for pareto-optimal neural architectures. In *ECCV*, 2018. 7

[19] Mark Everingham, Luc Van Gool, Christopher KI Williams, John Winn, and Andrew Zisserman. The pascal visual object classes (VOC) challenge. *IJCV*, 88(2):303–338, 2010. 1, 2

[20] Naiyu Gao, Yanhu Shan, Yupei Wang, Xin Zhao, Yinan Yu, Ming Yang, and Kaiqi Huang. Ssap: Single-shot instance segmentation with affinity pyramid. In *ICCV*, 2019. 2, 7, 8

[21] Shang-Hua Gao, Ming-Ming Cheng, Kai Zhao, Xin-Yu Zhang, Ming-Hsuan Yang, and Philip Torr. Res2net: A new multi-scale backbone architecture. *IEEE TPAMI*, 2020. 1, 2

[22] Ross Girshick, Jeff Donahue, Trevor Darrell, and Jitendra Malik. Rich feature hierarchies for accurate object detection and semantic segmentation. In *CVPR*, 2014. 1

[23] Ian Goodfellow, Yoshua Bengio, Aaron Courville, and Yoshua Bengio. *Deep learning*, volume 1. MIT press Cambridge, 2016. 1

[24] Priya Goyal, Piotr Dollár, Ross Girshick, Pieter Noordhuis, Lukasz Wesolowski, Aapo Kyrola, Andrew Tulloch, Yangqing Jia, and Kaiming He. Accurate, large minibatch sgd: Training imagenet in 1 hour. *arXiv preprint arXiv:1706.02677*, 2017. 1

[25] Song Han, Huizi Mao, and William J Dally. Deep compression: Compressing deep neural networks with pruning, trained quantization and huffman coding. In *ICLR*, 2016. 7

[26] Bharath Hariharan, Pablo Arbeláez, Ross Girshick, and Jitendra Malik. Simultaneous detection and segmentation. In *ECCV*, 2014. 1

[27] Kaiming He, Georgia Gkioxari, Piotr Dollár, and Ross Girshick. Mask r-cnn. In *ICCV*, 2017. 2

[28] Kaiming He, Xiangyu Zhang, Shaoqing Ren, and Jian Sun. Deep residual learning for image recognition. In *CVPR*, 2016. 1, 2, 6

[29] Kaiming He, Xiangyu Zhang, Shaoqing Ren, and Jian Sun. Identity mappings in deep residual networks. In *ECCV*, 2016. 2

[30] Xuming He, Richard S Zemel, and Miguel Á Carreira-Perpiñán. Multiscale conditional random fields for image labeling. In *CVPR*, 2004. 1

[31] Matthias Holschneider, Richard Kronland-Martinet, Jean Morlet, and Ph Tchamitchian. A real-time algorithm for signal analysis with the help of the wavelet transform. In *Wavelets: Time-Frequency Methods and Phase Space*, pages 289–297. Springer, 1989. 3

[32] Namdar Homayounfar, Yuwen Xiong, Justin Liang, Wei-Chiu Ma, and Raquel Urtasun. Levelset r-cnn: A deep variational method for instance segmentation. In *ECCV*, 2020. 3, 8

[33] Rui Hou, Jie Li, Arjun Bhargava, Allan Raventos, Vitor Guizilini, Chao Fang, Jerome Lynch, and Adrien Gaidon. Real-time panoptic segmentation from dense detections. In *CVPR*, 2020. 1, 7

[34] Andrew Howard, Mark Sandler, Grace Chu, Liang-Chieh Chen, Bo Chen, Mingxing Tan, Weijun Wang, Yukun Zhu, Ruoming Pang, Vijay Vasudevan, et al. Searching for mobilenetv3. In *ICCV*, 2019. 2, 3, 6

[35] Andrew G Howard, Menglong Zhu, Bo Chen, Dmitry Kalenichenko, Weijun Wang, Tobias Weyand, Marco Andreetto, and Hartwig Adam. Mobilenets: Efficient convolutional neural networks for mobile vision applications. *arXiv:1704.04861*, 2017. 2, 3, 5

[36] Jie Hu, Li Shen, and Gang Sun. Squeeze-and-excitation networks. In *CVPR*, 2018. 1, 2, 3

[37] Gao Huang, Zhuang Liu, Laurens Van Der Maaten, and Kilian Q Weinberger. Densely connected convolutional networks. In *CVPR*, 2017. 2

[38] Gao Huang, Yu Sun, Zhuang Liu, Daniel Sedra, and Kilian Q Weinberger. Deep networks with stochastic depth. In *ECCV*, 2016. 5

[39] Yanping Huang, Yonglong Cheng, Dehao Chen, HyoukJoong Lee, Jiquan Ngiam, Quoc V Le, and Zhifeng Chen. GPipe: Efficient training of giant neural networks using pipeline parallelism. In *NeurIPS*, 2019. 2

[40] Sergey Ioffe and Christian Szegedy. Batch normalization: accelerating deep network training by reducing internal covariate shift. In *ICML*, 2015. 1, 2, 4

[41] Alex Kendall, Yarin Gal, and Roberto Cipolla. Multi-task learning using uncertainty to weigh losses for scene geometry and semantics. In *CVPR*, 2018. 2

[42] Diederik P Kingma and Jimmy Ba. Adam: a method for stochastic optimization. In *ICLR*, 2015. 1, 4

[43] Alexander Kirillov, Ross Girshick, Kaiming He, and Piotr Dollár. Panoptic feature pyramid networks. In *CVPR*, 2019. 2, 7

[44] Alexander Kirillov, Kaiming He, Ross Girshick, Carsten Rother, and Piotr Dollár. Panoptic segmentation. In *CVPR*, 2019. 1, 2, 3

[45] Alexander Kolesnikov, Lucas Beyer, Xiaohua Zhai, Joan Puigcerver, Jessica Yung, Sylvain Gelly, and Neil Houlsby. Big transfer (bit): General visual representation learning. In *ECCV*, 2020. 2

[46] Alex Krizhevsky, Ilya Sutskever, and Geoffrey E. Hinton. Imagenet classification with deep convolutional neural networks. In *NeurIPS*, 2012. 1, 2

[47] Justin Lazarow, Kwonjoon Lee, Kunyu Shi, and Zhuowen Tu. Learning instance occlusion for panoptic segmentation. In *CVPR*, 2020. 2

[48] Yann LeCun, Léon Bottou, Yoshua Bengio, and Patrick Haffner. Gradient-based learning applied to document recognition. *Proceedings of the IEEE*, 86(11):2278–2324, 1998. 2

[49] Dong-Hyun Lee. Pseudo-label: The simple and efficient semi-supervised learning method for deep neural networks. In *ICML Workshop*, 2013. 6

[50] Youngwan Lee and Jongyoul Park. Centermask: Real-time anchor-free instance segmentation. In *CVPR*, 2020. 3

[51] Jie Li, Allan Raventos, Arjun Bhargava, Takaaki Tagawa, and Adrien Gaidon. Learning to fuse things and stuff. *arXiv:1812.01192*, 2018. 2, 5, 7, 8

[52] Qizhu Li, Xiaojuan Qi, and Philip HS Torr. Unifying training and inference for panoptic segmentation. In *CVPR*, 2020. 2, 7, 8

[53] Xiangtai Li, Xia Li, Li Zhang, Guangliang Cheng, Jianping Shi, Zhouchen Lin, Shaohua Tan, and Yunhai Tong. Improving semantic segmentation via decoupled body and edge supervision. In *ECCV*, 2020. 3, 8

[54] Xiang Li, Wenhai Wang, Xiaolin Hu, and Jian Yang. Selective kernel networks. In *CVPR*, 2019. 1, 2

[55] Yanwei Li, Xinze Chen, Zheng Zhu, Lingxi Xie, Guan Huang, Dalong Du, and Xingang Wang. Attention-guided unified network for panoptic segmentation. In *CVPR*, 2019. 2, 7

[56] Justin Liang, Namdar Homayounfar, Wei-Chiu Ma, Yuwen Xiong, Rui Hu, and Raquel Urtasun. Polytransform: Deep polygon transformer for instance segmentation. In *CVPR*, 2020. 3, 8

[57] Tsung-Yi Lin, Michael Maire, Serge Belongie, James Hays, Pietro Perona, Deva Ramanan, Piotr Dollár, and C Lawrence Zitnick. Microsoft coco: Common objects in context. In *ECCV*, 2014. 1, 2, 4

[58] Chenxi Liu, Liang-Chieh Chen, Florian Schroff, Hartwig Adam, Wei Hua, Alan Yuille, and Li Fei-Fei. Auto-DeepLab: Hierarchical neural architecture search for semantic image segmentation. In *CVPR*, 2019. 2, 8

[59] Shu Liu, Lu Qi, Haifang Qin, Jianping Shi, and Jiaya Jia. Path aggregation network for instance segmentation. In *CVPR*, 2018. 8

[60] Wei Liu, Andrew Rabinovich, and Alexander C Berg. Parsenet: Looking wider to see better. *arXiv:1506.04579*, 2015. 4

[61] Huanyu Liu1, Chao Peng, Changqian Yu, Jingbo Wang, Xu Liu, Gang Yu, and Wei Jiang. An end-to-end network for panoptic segmentation. In *CVPR*, 2019. 2

[62] Jonathan Long, Evan Shelhamer, and Trevor Darrell. Fully convolutional networks for semantic segmentation. In *IEEE TPAMI*, 2015. 1, 2

[63] Ningning Ma, Xiangyu Zhang, Hai-Tao Zheng, and Jian Sun. Shufflenet v2: Practical guidelines for efficient cnn architecture design. In *ECCV*, 2018. 2

[64] Gerhard Neuhold, Tobias Ollmann, Samuel Rota Bulò, and Peter Kontschieder. The mapillary vistas dataset for semantic understanding of street scenes. In *ICCV*, 2017. 1, 3, 4, 6

[65] Davy Neven, Bert De Brabandere, Marc Proesmans, and Luc Van Gool. Instance segmentation by jointly optimizing spatial embeddings and clustering bandwidth. In *CVPR*, 2019. 2

[66] George Papandreou, Iasonas Kokkinos, and Pierre-Andre Savalle. Modeling local and global deformations in deep learning: Epitomic convolution, multiple instance learning, and sliding window detection. In *CVPR*, 2015. 3

[67] Chao Peng, Tete Xiao, Zeming Li, Yuning Jiang, Xiangyu Zhang, Kai Jia, Gang Yu, and Jian Sun. Megdet: A large mini-batch object detector. In *CVPR*, 2018. 1

[68] Lorenzo Porzi, Samuel Rota Bulò, Aleksander Colovic, and Peter Kontschieder. Seamless scene segmentation. In *CVPR*, 2019. 2, 5, 7, 8

[69] Haozhi Qi, Zheng Zhang, Bin Xiao, Han Hu, Bowen Cheng, Yichen Wei, and Jifeng Dai. Deformable convolutional networks – COCO detection and segmentation challenge 2017 entry. *ICCV COCO Challenge Workshop*, 2017. 2, 6

[70] Siyuan Qiao, Liang-Chieh Chen, and Alan Yuille. Detectors: Detecting objects with recursive feature pyramid and switchable atrous convolution. *arXiv:2006.02334*, 2020. 2, 3, 5, 7

[71] Siyuan Qiao, Huiyu Wang, Chenxi Liu, Wei Shen, and Alan Yuille. Weight standardization. *arXiv:1903.10520*, 2019. 1

[72] Ilija Radosavovic, Raj Prateek Kosaraju, Ross Girshick, Kaiming He, and Piotr Dollár. Designing network design spaces. In *CVPR*, 2020. 1, 2

[73] Shaoqing Ren, Kaiming He, Ross Girshick, and Jian Sun. Faster R-CNN: Towards real-time object detection with region proposal networks. In *NeurIPS*, 2015. 1

[74] Samuel Rota Bulò, Lorenzo Porzi, and Peter Kontschieder. In-place activated batchnorm for memory-optimized training of dnns. In *CVPR*, 2018. 3

[75] Olga Russakovsky, Jia Deng, Hao Su, Jonathan Krause, Sanjeev Satheesh, Sean Ma, Zhiheng Huang, Andrej Karpathy, Aditya Khosla, Michael Bernstein, Alexander C. Berg, and Li Fei-Fei. ImageNet Large Scale Visual Recognition Challenge. *IJCV*, 2015. 1, 2

[76] Tim Salimans and Durk P Kingma. Weight normalization: A simple reparameterization to accelerate training of deep neural networks. In *NeurIPS*, 2016. 1

[77] Mark Sandler, Andrew Howard, Menglong Zhu, Andrey Zhmoginov, and Liang-Chieh Chen. Mobilenetv2: Inverted residuals and linear bottlenecks. In *CVPR*, 2018. 2, 7

[78] Pierre Sermanet, David Eigen, Xiang Zhang, Michaël Mathieu, Rob Fergus, and Yann LeCun. Overfeat: Integrated recognition, localization and detection using convolutional networks. In *ICLR*, 2014. 2

[79] Karen Simonyan and Andrew Zisserman. Very deep convolutional networks for large-scale image recognition. In *ICLR*, 2015. 1, 2

[80] Konstantin Sofiiuk, Olga Barinova, and Anton Konushin. Adaptis: Adaptive instance selection network. In *ICCV*, 2019. 7, 8

[81] Ke Sun, Yang Zhao, Borui Jiang, Tianheng Cheng, Bin Xiao, Dong Liu, Yadong Mu, Xinggang Wang, Wenyu Liu, and Jingdong Wang. High-resolution representations for labeling pixels and regions. *arXiv:1904.04514*, 2019. 8

[82] Christian Szegedy, Sergey Ioffe, Vincent Vanhoucke, and Alexander A Alemi. Inception-v4, inception-resnet and the impact of residual connections on learning. In *AAAI*, 2017. 2

[83] Christian Szegedy, Vincent Vanhoucke, Sergey Ioffe, Jon Shlens, and Zbigniew Wojna. Rethinking the inception architecture for computer vision. In *CVPR*, 2016. 2

[84] Towaki Takikawa, David Acuna, Varun Jampani, and Sanja Fidler. Gated-scnn: Gated shape cnns for semantic segmentation. In *ICCV*, 2019. 3

[85] Mingxing Tan, Bo Chen, Ruoming Pang, Vijay Vasudevan, Mark Sandler, Andrew Howard, and Quoc V Le. Mnasnet: Platform-aware neural architecture search for mobile. In *CVPR*, 2019. 7

[86] Mingxing Tan and Quoc V Le. EfficientNet: Rethinking model scaling for convolutional neural networks. In *ICML*, 2019. 2, 3

[87] Mingxing Tan, Ruoming Pang, and Quoc V Le. Efficientdet: Scalable and efficient object detection. In *CVPR*, 2020. 2

[88] Jonas Uhrig, Eike Rehder, Björn Fröhlich, Uwe Franke, and Thomas Brox. Box2pix: Single-shot instance segmentation by assigning pixels to object boxes. In *IEEE Intelligent Vehicles Symposium (IV)*, 2018. 2

[89] Haochen Wang, Ruotian Luo, Michael Maire, and Greg Shakhnarovich. Pixel consensus voting for panoptic segmentation. In *CVPR*, 2020. 1, 2, 7

[90] Huiyu Wang, Yukun Zhu, Bradley Green, Hartwig Adam, Alan Yuille, and Liang-Chieh Chen. Axial-deeplab: Standalone axial-attention for panoptic segmentation. In *ECCV*, 2020. 2, 6, 7, 8

[91] Panqu Wang, Pengfei Chen, Ye Yuan, Ding Liu, Zehua Huang, Xiaodi Hou, and Garrison Cottrell. Understanding convolution for semantic segmentation. *arXiv:1702.08502*, 2017. 5

[92] Yuxin Wu and Kaiming He. Group normalization. In *ECCV*, 2018. 1

[93] Yangxin Wu, Gengwei Zhang, Yiming Gao, Xiajun Deng, Ke Gong, Xiaodan Liang, and Liang Lin. Bidirectional graph reasoning network for panoptic segmentation. In *CVPR*, 2020. 2, 6, 8

[94] Yangxin Wu, Gengwei Zhang, Hang Xu, Xiaodan Liang, and Liang Lin. Auto-panoptic: Cooperative multi-component architecture search for panoptic segmentation. In *NeurIPS*, 2020. 2, 6, 8

[95] Zifeng Wu, Chunhua Shen, and Anton Van Den Hengel. Wider or deeper: Revisiting the ResNet model for visual recognition. *Pattern Recognition*, 2019. 1, 2, 3, 7

[96] Qizhe Xie, Eduard Hovy, Minh-Thang Luong, and Quoc V Le. Self-training with noisy student improves imagenet classification. *arXiv:1911.04252*, 2019. 6

[97] Saining Xie, Ross Girshick, Piotr Dollár, Zhuowen Tu, and Kaiming He. Aggregated residual transformations for deep neural networks. In *CVPR*, 2017. 1, 2

[98] Yuwen Xiong, Renjie Liao, Hengshuang Zhao, Rui Hu, Min Bai, Ersin Yumer, and Raquel Urtasun. UPSNet: A unified panoptic segmentation network. In *CVPR*, 2019. 1, 2, 5, 7, 8

[99] Tien-Ju Yang, Maxwell D Collins, Yukun Zhu, Jyh-Jing Hwang, Ting Liu, Xiao Zhang, Vivienne Sze, George Papandreou, and Liang-Chieh Chen. DeeperLab: Single-shot image parser. *arXiv:1902.05093*, 2019. 1, 2, 7, 8

[100] Tien-Ju Yang, Andrew Howard, Bo Chen, Xiao Zhang, Alec Go, Mark Sandler, Vivienne Sze, and Hartwig Adam. Netadapt: Platform-aware neural network adaptation for mobile applications. In *ECCV*, 2018. 7

[101] Yibo Yang, Hongyang Li, Xia Li, Qijie Zhao, Jianlong Wu, and Zhouchen Lin. Sognet: Scene overlap graph network for panoptic segmentation. In *AAAI*, 2020. 7

[102] Changqian Yu, Jingbo Wang, Changxin Gao, Gang Yu, Chunhua Shen, and Nong Sang. Context prior for scene segmentation. In *CVPR*, 2020. 8

[103] Yuhui Yuan, Xilin Chen, and Jingdong Wang. Object-contextual representations for semantic segmentation. In *ECCV*, 2020. 8

[104] Yuhui Yuan, Jingyi Xie, Xilin Chen, and Jingdong Wang. Segfix: Model-agnostic boundary refinement for segmentation. In *ECCV*, 2020. 8

[105] Sergey Zagoruyko and Nikos Komodakis. Wide residual networks. In *BMVC*, 2016. 1, 2, 3, 7

[106] Hang Zhang, Chongruo Wu, Zhongyue Zhang, Yi Zhu, Zhi Zhang, Haibin Lin, Yue Sun, Tong He, Jonas Mueller, R Manmatha, et al. Resnest: Split-attention networks. *arXiv:2004.08955*, 2020. 1, 2

[107] Hengshuang Zhao, Jianping Shi, Xiaojuan Qi, Xiaogang Wang, and Jiaya Jia. Pyramid scene parsing network. In *CVPR*, 2017. 2, 6, 8

[108] Bolei Zhou, Hang Zhao, Xavier Puig, Tete Xiao, Sanja Fidler, Adela Barriuso, and Antonio Torralba. Semantic understanding of scenes through the ade20k dataset. *IJCV*, 2019. 4

[109] Yi Zhu, Karan Sapra, Fitsum A Reda, Kevin J Shih, Shawn Newsam, Andrew Tao, and Bryan Catanzaro. Improving semantic segmentation via video propagation and label relaxation. In *CVPR*, 2019. 3, 6, 8